Signal Processing 98 (2014) 252–262

Contents lists available at ScienceDirect

Signal Processing

journal homepage: www.elsevier.com/locate/sigpro

A novel covariation based noncircular sources direction finding method under impulsive noise environments

Zhang Jinfeng [a,b], Qiu Tianshuang [b,*]

[a] Shenzhen Key Lab of Advanced Communications and Information Processing, Shenzhen University, Shenzhen 518060, China
[b] Faculty of Electronic Information and Electrical Engineering, Dalian University of Technology, Dalian 116024, China

ARTICLE INFO

Article history:
Received 1 February 2013
Received in revised form
26 November 2013
Accepted 28 November 2013
Available online 6 December 2013

Keywords:
MUSIC
Noncircular
Covariation
Complex symmetric alpha-stable

ABSTRACT

We extend the bearing estimation method for noncircular signals to the impulsive noise scenario which can be modeled as a complex symmetric alpha-stable ($S\alpha S$) process. We define the extended covariation based matrix of the sensor outputs and show that it can be applied with subspace techniques to extract the bearing information from noncircular sources. Comprehensive simulations demonstrate that the proposed direction finding algorithm outperforms the traditional NC-MUSIC algorithm in the presence of a wide range of impulsive noise environments.

1. Introduction

Subspace-based methods have been the dominant techniques for estimating the directions of arrival (DOA) of narrowband sources which impinge on an array of sensors [1–3], i.e., the well known eigendecomposition based MUSIC algorithm is to obtain the high-resolution direction estimates by exploiting the orthogonality between a sample subspace and a DOA parameter-dependent subspace [2]. However, there are two distinct disadvantages in the traditional MUSIC algorithm. Firstly, it is not capable of processing more than $M-1$ noncoherent incoming signals from an array of M sensors. Secondly, it is designed to be limited to extracting the bearing information from complex circular signals; that is, for noncircular signals, it suffers from model mismatch and degrades dramatically in its performance.

In recent years, developing direction finding methods for noncircular signals, e.g., binary phased-shift keying (BPSK), offset-quadrature-phase-shift keying (OQPSK) modulated signals, has aroused plenty of interest through exploiting the inherent potentials of noncircular signals. By conducting eigendecomposition on the extended covariance matrix, in which the conventional covariance function is employed in company with the unconjugated spatial covariance function, for the sensor outputs, Gounon proposed the NC-MUSIC algorithm [4]. In Ref. [5], Chargé improved the computation procedure of NC-MUSIC by using a polynomial rooting technique, and proposed the so-called NC-root-MUSIC algorithm. Haardt [6] and Zoubir [7] extended the classic ESPRIT method and proposed the ESPRIT-like algorithms for noncircular signals. The asymptotic performance of the MUSIC-like algorithms has been investigated in Ref. [8]. In comparison with the traditional MUSIC and ESPRIT methods, the maximum number of sources that can be processed has been increased in all the above algorithms and the estimation accuracy has been improved significantly as well. Moreover, high-order cumulants have been explored and the so-called extended 2q-MUSIC algorithm has been proposed in Ref. [9] for noncircular sources localization, by which the array aperture has been extended further [9].

* Corresponding author. Tel.: +86 411 84706009; fax: +86 411 84709573.
E-mail address: qiutsh@dlut.edu.cn (Q. Tianshuang).

0165-1684/$ - see front matter © 2013 Elsevier B.V. All rights reserved.
http://dx.doi.org/10.1016/j.sigpro.2013.11.031

Despite the advantages of these algorithms, they also have limitations. These algorithms have been studied under the assumption of Gaussian or second-order model. The utilization of second order or higher order statistics, e.g., covariance, unconjugated covariance, and higher order cumulants, has been the major methodology of these algorithms by assuming that the additive noise is Gaussian distributed. However, for a fairly common case, it is inappropriate to model the noise as Gaussian. Recent studies show that in some scenarios, sudden bursts or sharp spikes are exhibited at the array outputs which can be characterized as impulsive due to clutter sources such as mountains, forests and sea waves [10–12]. This impulsive component of noise has been found to be significant in many problems, including atmospheric noise and underwater problems such as sonar and submarine communication. Taking these scenarios into account, we are interested in developing direction finding methods for noncircular signals suitable for not only Gaussian but also impulsive noise environments.

Researchers have studied this impulsive nature and shown that the symmetric alpha stable ($S\alpha S$) processes are better models for impulsive noise than the Gaussian processes [13–15]. The real $S\alpha S$ process can be defined by its characteristic function $\varphi(\omega)=\exp(ja\omega-\gamma|\omega|^{\alpha})$. Where α is the characteristic exponent taking values $0<\alpha\le 2$, and γ is the dispersion which is similar to the variance of the Gaussian distribution. Specially, Gaussian processes are stable processes with $\alpha=2$. For these distributions with $\alpha<2$, they present heavier tails than those of Gaussian distribution and possess finite pth-order moments only for $p<\alpha<2$. These processes satisfy the stability property which states that linear combinations of jointly stable variables are indeed stable. They arise as limiting processes of sums of i.i.d random variables via the generalized central limit theorem. For details about $S\alpha S$ processes, see Ref. [15], and the references therein.

Due to the lack of finite variance, covariances do not exist on the space of $S\alpha S$ random variables. Instead, the quantity covariation plays a role for $S\alpha S$ random variables analogous to the one played by covariance for Gaussian random variables [16]. In this paper, we address the direction finding problem in the presence of impulsive noise by utilizing the extended covariation based matrix of the sensor outputs for noncircular sources. This paper is organized as follows: In Section 2, we present some necessary information on covariation. In Section 3, we define the problem of interest. In Section 4, we propose a new subspace algorithm based on covariation for noncircular sources. Finally, simulation experiments are presented in Section 5, and conclusions are drawn in Section 6.

The following notations are utilized throughout this paper. The superscripts "T", "H" and "$*$" denote the transpose, the conjugate transpose, and the conjugate, respectively. $E(\cdot)$, $\|\cdot\|_{\mathrm{Fro}}$, $\Re(\cdot)$ and $\Im(\cdot)$ stand for the expectation, Frobenius norm, and real and imaginary part operators, respectively. $\mathbf{I_M}$ is the $M\times M$ identity matrix.

2. Covariation and its properties

A complex random variable (RV) $X=X_1+jX_2$ is $S\alpha S$ if X_1 and X_2 are jointly $S\alpha S$. Several complex RV's are jointly $S\alpha S$ if their real and imaginary parts are jointly $S\alpha S$ [15]. When $X=X_1+jX_2$ and $Y=Y_1+jY_2$ are jointly $S\alpha S$ with $1<\alpha\le 2$, the covariation of X and Y is defined by

$$[X,Y]_{\alpha}=\frac{E\{XY^{\langle p-1\rangle}\}}{E\{|Y|^{p}\}}\gamma_Y \quad 1\le p<\alpha \tag{1}$$

where $Y^{\langle b\rangle}=|Y|^{b-1}Y^{*}$ and γ_Y is the dispersion of RV, Y given by

$$\gamma_Y^{p/\alpha}=\frac{E\{|Y|^{p}\}}{C(p,\alpha)} \quad \text{for } 0<p<\alpha \tag{2}$$

with

$$C(p,\alpha)=\frac{2^{p+1}\Gamma(p+2/2)\Gamma(-p/\alpha)}{\alpha\Gamma(1/2)\Gamma(-p/2)}, \tag{3}$$

in which $\Gamma(\cdot)$ is the gamma function defined by

$$\Gamma(x)=\int_0^{\infty}t^{x-1}e^{-t}\,dt \tag{4}$$

Also, the covariation coefficient of X and Y is defined by

$$\lambda_{X,Y}=\frac{[X,Y]_{\alpha}}{[Y,Y]_{\alpha}} \tag{5}$$

and by using (1), it can be expressed as

$$\lambda_{X,Y}=\frac{E\{XY^{\langle p-1\rangle}\}}{E\{|Y|^{p}\}} \quad \text{for } 1\le p<\alpha \tag{6}$$

Next, we list three main properties of covarition of complex jointly $S\alpha S$ RV's as follows:

P1. The covariation $[X,Y]_{\alpha}$ is linear in X, that is, if X_1, X_2, Y are jointly $S\alpha S$ then

$$[\beta_1X_1+\beta_2X_2,Y]_{\alpha}=\beta_1[X_1,Y]_{\alpha}+\beta_2[X_2,Y]_{\alpha} \tag{7}$$

for any complex constants β_1 and β_2.

P2. $[X,Y]_{\alpha}$ possesses the following pseudo-linearity property with respect to Y, that is, if Y_1, Y_2 are independent and X, Y_1, Y_2 are jointly $S\alpha S$, then

$$[X,\xi_1Y_1+\xi_2Y_2]_{\alpha}=\xi_1^{\langle\alpha-1\rangle}[X,Y_1]_{\alpha}+\xi_2^{\langle\alpha-1\rangle}[X,Y_2]_{\alpha} \tag{8}$$

for any complex constants ξ_1 and ξ_2.

P3. If X and Y are independent $S\alpha S$, then $[X,Y]_{\alpha}=0$.

3. Problem formulation

3.1. Array model

Assume P narrow-band independent, complex isotropic $S\alpha S$ $(1<\alpha\le 2)$ signals with locations $\{\theta_1,\theta_2,\ldots,\theta_P\}$ are impinging on a uniformly linear array of M sensors. The underlying noises are i.i.d. isotropic complex $S\alpha S$ random processes with the same characteristic exponent α as the signals. In addition, we also assume that the real parts and the imaginary parts of the complex $S\alpha S$ noises are independent with each other [4–7]. Using the complex envelope representation, the array output can be expressed as

$$x_m(t)=\sum_{k=1}^{P}a(\theta_k)s_k(t)+n_m(t), \quad m=1,2,\ldots,M \tag{9}$$

where $a(\theta_k)=e^{-j(2\pi/\lambda)(m-1)d\,\sin(\theta_k)}$ is the steering coefficient of the mth sensor toward direction θ_k, λ denotes the

wavelength of the carrier and d is the distance between two sensors, $s_k(t)$ is the kth signal received at the reference sensor, and $n_m(t)$ is the underlying noise at sensor $x_m(t)$.

The vector form of (9) can be expressed as

$$\mathbf{x}(t)=A(\theta)\mathbf{s}(t)+\mathbf{n}(t) \tag{10}$$

where $\mathbf{A}(\boldsymbol{\theta})$ is the $M\times P$ matrix of the array steering vectors $\mathbf{A}(\boldsymbol{\theta})=[\mathbf{a}(\theta_1),\mathbf{a}(\theta_2),\ldots,\mathbf{a}(\theta_p)]$, in which $\mathbf{a}(\theta_k)=[1, e^{-j(2\pi/\lambda)d\ \sin(\theta_k)},\ldots, e^{-j(2\pi/\lambda)d(M-1)\sin(\theta_k)}]^T$, $\mathbf{x}(t)$ is the $M\times 1$ vector of signals received by the array sensors $\mathbf{x}(t)=[x_1(t), x_2(t),\ldots,x_M(t)]^T$, $\mathbf{s}(t)$ is the $P\times 1$ vector of the signals $\mathbf{s}(t)=[s_1(t),s_2(t),\ldots,s_p(t)]^T$, and $\mathbf{n}(t)$ is the $M\times 1$ vector of the noise $\mathbf{n}(t)=[n_1(t),n_2(t),\ldots,n_M(t)]^T$.

3.2. Noncircular signals

Circularity can be derived from the geometrical interpretation of signals [17]. A complex random variable is said to be circular if its statistical properties are rotational invariant for an arbitrary phase ψ. In this paper, we only consider the first and the second order statistical properties of the signals. A complex random signal z is said to be circular at the order 2 if both of the mean $E\{z\}$ and the elliptic covariance $E\{z^2\}$ equal zero. Since the signals are often assumed to be zero-mean, the noncircularity of z can be equated to $E\{z^2\}\neq 0$. Circularity is a common hypothesis for the narrowband signals in the classic direction finding algorithms, but we still can easily find numerous noncircular signals like AM (amplitude modulated) or BPSK signals.

For an arbitrary signal z, we acquire

$$E\{z^2\}=\rho e^{j\phi}E\{zz^*\}=\rho e^{j\phi}\sigma_z^2 \tag{11}$$

where ϕ is the noncircularity phase and ρ is the noncircularity rate which satisfies $0\le\rho\le 1$. Obviously, circular signal is the special case with $\rho=0$. In this paper, we consider only the noncircular signals with $\rho=1$, e.g., BPSK and AM signals. In this case, the noncircular signal z can be expressed as [6]

$$z=e^{(j\phi/2)}z_0 \tag{12}$$

where z_0 is the zero phase version of z.

Therefore, for the noncircular signal z, we can incorporate the unconjugated spatial covariance function $E\{z^2\}$ with the conventional covariance function $E\{zz^*\}$ to gain more abundant second order statistical information.

4. Proposed solution in the $S\alpha S$ framework

4.1. The extended covariation based NC-MUSIC algorithm

In this section, we will derive the extended covariation based matrix of the sensor outputs and show it can be applied with subspace techniques to gain the bearing information for noncircular sources under $S\alpha S$ noise environments.

Considering the noncircular signals with the noncircularity rate $\rho=1$, from Eq. (12), we can describe the signal $\mathbf{s}(t)$ in Eq. (10) as

$$\mathbf{s}(t)=\Phi^{1/2}\mathbf{s}_0(t) \tag{13}$$

where $\mathbf{s}_0(t)=[s_{01}(t),s_{02}(t),\ldots,s_{0P}(t)]^T$, in which the $\{s_{0i}(t)\}_{i=1}^P$ is the corresponding zero phase version of the signal $\{s_i(t)\}_{i=1}^P$, and $\Phi^{1/2}=\mathrm{diag}\{e^{j\phi_1/2}, e^{j\phi_2/2},\ldots, e^{j\phi_p/2}\}$, in which $\{\phi_i\}_{i=1}^P$ is representing the noncircularity phase of the signal $\{s_i(t)\}_{i=1}^P$. Suppose only noncircular signals are involved in $\mathbf{s}(t)$, we can form the extended array output $\mathbf{x}_{nc}(t)$ as the combination of $\mathbf{x}(t)$ and its conjugate version $\mathbf{x}^*(t)$

$$\mathbf{x}_{\mathrm{nc}}(t)=\begin{bmatrix}\mathbf{x}(t)\\ \mathbf{x}^*(t)\end{bmatrix} \tag{14}$$

Definition 1. The $2M\times 2M$ extended covariation matrix $\mathbf{C}_{nc}$ of the extended output vector $\mathbf{x}_{nc}(t)$ can be defined as

$$\mathbf{C}_{nc}=\begin{bmatrix}\mathbf{C}^1 & \mathbf{C}^2\\ \mathbf{C}^3 & \mathbf{C}^4\end{bmatrix} \tag{15}$$

where $\mathbf{C}^1$, $\mathbf{C}^2$, $\mathbf{C}^3$, and $\mathbf{C}^4$ are the four $M\times M$ sub-matrices of $\mathbf{C}_{nc}$, and the corresponding (i,j)th entries of these sub-matrices are taking the values $[x_i(t),x_j(t)]_\alpha$, $[x_i(t),x_j^*(t)]_\alpha$, $[x_i^*(t),x_j(t)]_\alpha$ and $[x_i^*(t),x_j^*(t)]_\alpha$, respectively.

Theorem 1. The matrix form $\mathbf{C}_{nc}$ can be expressed as

$$\mathbf{C}_{\mathrm{nc}}=\begin{bmatrix}\mathbf{A} & \mathbf{0}\\ \mathbf{0} & \mathbf{A}^*\end{bmatrix}\begin{bmatrix}\Gamma_{0\mathbf{s}} & \mathbf{0}\\ \mathbf{0} & \Gamma_{0\mathbf{s}}\end{bmatrix}\begin{bmatrix}\mathbf{I}_{\mathrm{P}} & \Phi\\ \Phi^* & \mathbf{I}_{\mathrm{P}}\end{bmatrix}\begin{bmatrix}\mathbf{A} & \mathbf{0}\\ \mathbf{0} & \mathbf{A}^*\end{bmatrix}^H+\kappa_n\mathbf{I}_{2M} \tag{16}$$

where $\boldsymbol{\Gamma}_{0\mathbf{s}}=\mathrm{diag}\{\gamma_{01},\gamma_{02},\ldots,\gamma_{0P}\}$ is the diagonal covariation matrix for the signal $\mathbf{s}(t)$, in which $\gamma_{0k}=[s_{0k}(t),s_{0k}(t)]_\alpha$ $k=1,2,\ldots,P$. $\kappa_n=[n_i(t),n_i(t)]_\alpha$ $i=1,2,\ldots,M$ is the covariation of the noise. See Appendix A for the proof of Theorem 1.

We can further simplify the expression (16) as

$$\mathbf{C}_{nc}=\begin{bmatrix}\mathbf{A}\\ \mathbf{A}^*\Phi^*\end{bmatrix}\Gamma_{0\mathbf{s}}\begin{bmatrix}\mathbf{A}\\ \mathbf{A}^*\Phi^*\end{bmatrix}^H+\kappa_n\mathbf{I}_{2M} \tag{17}$$

Clearly, the expression for the extended covariation matrix $\mathbf{C}_{nc}$ is identical to the well-known expression $\mathbf{R}_{nc}$ which stands for the extended covariance matrix in NC-MUSIC [4]

$$\mathbf{R}_{nc}=\begin{bmatrix}\mathbf{A}\\ \mathbf{A}^*\Phi^*\end{bmatrix}\mathbf{R}_{0\mathbf{s}}\begin{bmatrix}\mathbf{A}\\ \mathbf{A}^*\Phi^*\end{bmatrix}^H+\sigma_n^2\mathbf{I}_{2M} \tag{18}$$

where $\mathbf{R}_{0\mathbf{s}}$ is the diagonal signal covariance matrix and σ_n^2 is the variance of the underlying noise.

Accordingly, similar to NC-MUSIC, we can formulate the extended steering vector

$$\mathbf{B}=\begin{bmatrix}\mathbf{A}\\ \mathbf{A}^*\Phi^*\end{bmatrix}=[\mathbf{b}(\theta_1,\phi_1),\mathbf{b}(\theta_2,\phi_2),\ldots,\mathbf{b}(\theta_P,\phi_P)] \tag{19}$$

where $\mathbf{b}(\theta_i,\phi_i)=[\,\mathbf{a}(\theta_i)\quad \mathbf{a}^*(\theta_i)e^{-j\phi_i}\,]^T\quad i=1,2,\cdots,P$. The DOAs can be obtained by minimizing the following spatial spectrum $g(\theta,\phi)$ over θ and ϕ

$$g(\theta,\phi)=\mathbf{b}^H(\theta,\phi)\mathbf{V}_n\mathbf{V}_n^H\mathbf{b}(\theta,\phi), \tag{20}$$

in which $\mathbf{V}_n$ are the corresponding left singular vectors associated with the noise subspace of $\mathbf{C}_{nc}$. To alleviate the computational complexity, like NC-MUSIC, the 2-D search of $g(\theta,\phi)$ over θ and ϕ can be substituted with the 1-D search only over θ for the local minima of the following

spectrum [4]

$$f(\theta)=\mathbf{a}^H(\theta)\mathbf{V}_{n1}\mathbf{V}_{n1}^H\mathbf{a}(\theta)+\mathbf{a}^T(\theta)\mathbf{V}_{n2}\mathbf{V}_{n2}^H\mathbf{a}^*(\theta)-2\|\mathbf{a}^H(\theta)\mathbf{V}_{n1}\mathbf{V}_{n2}^H\mathbf{a}^*(\theta)\| \tag{21}$$

where $\mathbf{V}_{n1}$ and $\mathbf{V}_{n2}$ are derived by partitioning $\mathbf{V}_n$ into two sub-matrices with the same dimension as

$$\mathbf{V}_n=\begin{bmatrix}\mathbf{V}_{n1}\\ \mathbf{V}_{n2}\end{bmatrix} \tag{22}$$

See Appendix B for the derivation of $f(\theta)$ in (21).

4.2. The implementation of EXC-NC-MUSIC

As analyzed in Section 4.1, the extended covariation based MUSIC algorithm for noncircular sources' direction finding, as we call EXC-NC-MUSIC algorithm, can be implemented by the following three procedures.

Step 1. Compute the $2M\times 2M$ matrix $\mathbf{C}_{nc}$ in (15), the parameter p in the covariation functions can be directly chosen as $p=1$. The reason for doing this is interpreted in Section 5.
Step 2. Execute SVD on $\mathbf{C}_{nc}$ and construct the $2M\times(2M-P)$ matrix $\mathbf{V}_n$ in (20).
Step 3. Compute the corresponding spectrum $f(\theta)$ in (21) and select the P local minima of $f(\theta)$ as the estimates of DOAs $\{\theta_1,\theta_2,\ldots,\theta_P\}$.

In practice, the entries of $\mathbf{C}_{nc}$ which involves covariation functions have to be estimated from a finite number of array sensor measurements. Ref. [15] introduced two such estimators for covariation coefficients which are called the modified fractional lower order moment (MFLOM) estimator and the screened ratio (SCR) estimator. As recommended in Ref. [15], the MFLOM estimator is employed in this paper. Based on fractional lower order moments of the stable process, the MFLOM estimator can be defined as

$$\hat{\lambda}_{X,Y}(p)=\frac{\sum_{i=1}^{n}X_iY_i^{\langle p-1\rangle}}{\sum_{i=1}^{n}|Y_i|^p}\quad 0<p<\alpha \tag{23}$$

for independent complex observations $(X_1,Y_1),\ldots,(X_n,Y_n)$. Apparently, when $1\le p<\alpha$ the MFLOM can be considered as the estimate of the covariation coefficient $\lambda_{X,Y}$ defined in (6).

In the following content, we illustrate the influence of the parameter p to the performance of the MFLOM estimator by means of Monte-Carlo (MC) simulations. Two $S\alpha S$ random variables, X and Y, are generated by $X=c_1U_1+c_2U_2$ and $Y=d_1U_1+d_2U_2$, where U_1, U_2 are independent $S\alpha S$ variables. c_1, c_2, d_1, and d_2 are arbitrary constants. So the true covariation coefficient $\lambda_{X,Y}$ of X with Y can be obtained as

$$\lambda_{X,Y}=\frac{c_1d_1^{\langle\alpha-1\rangle}+c_2d_2^{\langle\alpha-1\rangle}}{|d_1|^\alpha+|d_2|^\alpha} \tag{24}$$

In our simulations, the characteristic exponent α varies from 1.1 to 2.0. For each α, 5000 independent samples of U_1 and U_2 are generated. c_1, c_2, d_1, and d_2 are set at $c_1=-0.2$, $c_2=0.1$, $d_1=0.1$, and $d_2=0.2$, respectively. Fig. 1 and Table 1 present the standard deviations and the means of the MFLOM estimates, respectively. As we can observe from Fig. 1, for the case of non-Gaussian stable signals $(1<\alpha<2)$, the values of p in the range $(1/2,\alpha/2)$ result into the smallest standard deviations. For Gaussian signals, the optimal value of p is 2 as expected, and in such case, the MFLOM estimator is simplified to the least-squares (LS) estimator. Table 1 demonstrates the consistent results with those demonstrated in Fig. 1 by means of the estimation means of the MFLOM estimates.

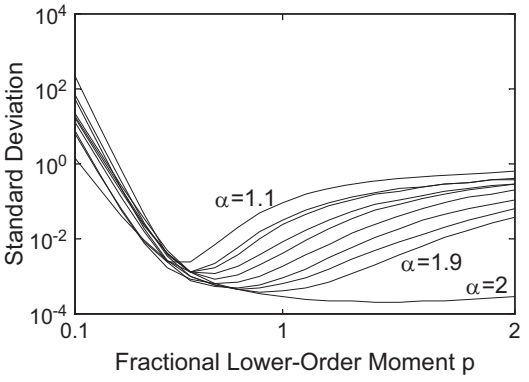

Fig. 1. The standard deviations of the MFLOM estimates as a function of the parameter p.

5. Simulations

In our simulations, we assume that statistically independent signals are received by a uniform linear array (ULA) sensors spaced half a wavelength apart. The underlying noises are isotropic complex $S\alpha S$ distributed and circular. Since a complex $S\alpha S$ random variable with $\alpha<2$ does not possess finite variance, the generalized signal-to-noise ratio (GSNR) which can be defined to evaluate the ratio of the signal power over noise dispersion γ by

Table 1
The means of the MFLOM estimates with several p values.

α	1.1	1.2	1.3	1.4	1.5	1.6	1.7	1.8	1.9	2.0
TRUE $\lambda_{X,Y}$	−0.2957	−0.2585	−0.2224	−0.1873	−0.1533	−0.1205	−0.0887	−0.0581	−0.0286	−0.0003
MFLOM ($p=0.1$)	−0.4318	0.2718	−0.5396	0.4655	−0.3264	−0.1185	0.0421	0.2417	−0.2172	0.1352
MFLOM ($p=0.5$)	−0.2987	−0.2578	−0.2246	−0.1774	−0.1593	−0.1169	−0.0869	−0.0612	−0.0389	0.0033
MFLOM ($p=0.9$)	−0.3047	−0.2511	−0.2147	−0.1696	−0.1590	−0.1210	−0.0854	−0.0604	−0.0300	0.0008
MFLOM ($p=2.0$)	−0.3303	−0.2896	−0.2592	−0.0512	−0.1344	−0.1530	−0.0502	−0.1049	-0.0153	0.0003

$\mathrm{GSNR}=10\log((1/\gamma K)\sum_{t=1}^{K}|s(t)|^2)$ is used to evaluate the signal-to-noise condition for finite sample realizations, where K represents the number of the available data samples.

In Section 5.1, we show the estimation capability of the proposed EXC-NC-MUSIC algorithm in two aspects: the aperture extension capability, and the capability of estimating DOAs for both noncircular signals and circular signals. In Section 5.2, we compare the performance of EXC-NC-MUSIC with NC-MUSIC and demonstrate the higher estimation precision of EXC-NC-MUSIC over NC-MUSIC in the presence of impulsive noise. It should be noted that the signals' types in the simulations in Sections 5.1 and 5.2 are those frequently encountered ones in practical communications applications, such as BPSK, QPSK, Gaussian, etc. In Section 5.3, we expand our simulation to the scenario which assumes that the signals and the noise are both $S\alpha S$ distributed but with different characteristic exponents. In Section 5.4, we discuss the selection of the parameter p for EXC-NC-MUSIC. The overall mathematical description of the signal types which have appeared in our simulations can be found in Appendix C.

Under the guidance of the discussions in Section 5.4, for all the experiments in Section 5, unless otherwise indicated, the parameter p in EXC-NC-MUSIC is directly set as a constant $p=1$.

5.1. Estimation capability

5.1.1. Aperture extension

EXC-NC-MUSIC can handle more noncircular signals than the number of sensors as NC-MUSIC. For the number of sensor array M, EXC-NC-MUSIC can handle $2(M-1)$ noncircular signals at most. Suppose four independent BPSK signals impinge on the 3 array sensors with the DOAs are $[-20^o,0^o,10^o,30^o]$. A moderate impulsive noise condition with $\alpha=1.6$ is employed. The GSNR is set to be 10 dB. The number of data samples available at each sensor is 300. Fig. 2 demonstrates 100 realizations of the estimation results of EXC-NC-MUSIC. It is evident from Fig. 2 that EXC-NC-MUSIC has the capability of aperture extension for noncircular signals as NC-MUSIC.

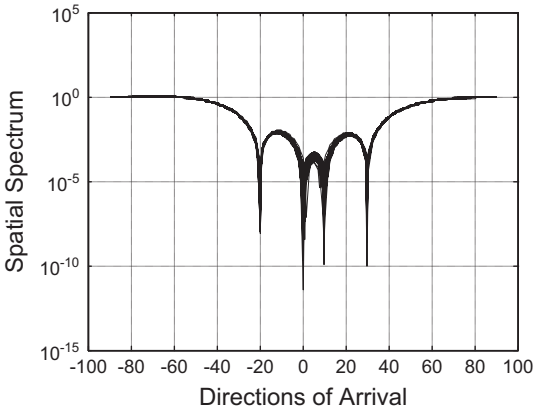

Fig. 2. The capability of aperture extension of EXC-NC-MUSIC.

5.1.2. Coexistence of both noncircular signals and circular signals

As NC-MUSIC, the proposed EXC-NC-MUSIC algorithm can gain the bearing information from not only noncircular signals but also circular signals. In this experiment, we assume four signals impinge on 5 array sensors, including two BPSK signals, one symmetrical Gaussian signal [19] and one QPSK (the quaternary-phase-shift keying) signal. The four independent signals come from -10°, 0°, 10° and 20°. The sources coming from -10° and 0° are supposed to send BPSK symbols, the source from 10° sends Gaussian symbols and the source from 20° sends QPSK symbols. The characteristic exponent of the noise is set at $\alpha=1.6$. The number of data samples available at each sensor is 1000. The GSNR employed for each signal is 15 dB.

Fig. 3(a) demonstrates the superposition of 100 realizations of the spatial spectrum of EXC-NC-MUSIC algorithm. As we can observe from Fig. 3(a), the EXC-NC-MUSIC can be applied for the DOA estimation under the coexistence of both noncircular and circular signals.

The performance in terms of root mean square error (RMSE) of EXC-NC-MUSIC under the coexistence of the four signals is displayed in Fig. 3(b). Where the RMSE of the DOA estimates for one source can be defined as $\mathrm{RMSE}\triangleq\sqrt{\frac{1}{L}\sum_{l=1}^{L}(\hat{\theta}(l)-\theta)^2}$, in which $\hat{\theta}(l)$ is the estimate of true DOA θ for the lth MC run and L is the total number of

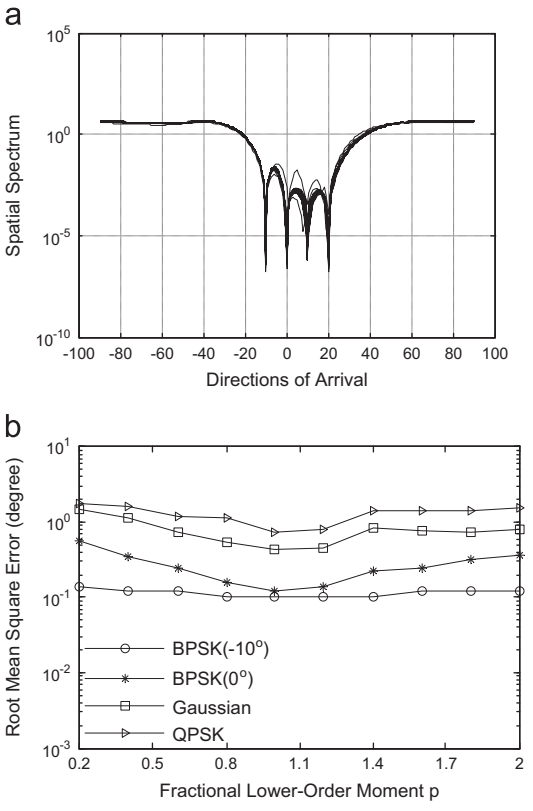

Fig. 3. The performance of EXC-NC-MUSIC under the coexistence of both noncircular and circular signals. (a) Spatial spectrum and (b) root mean square error.

the MC runs. It is noticed from Fig. 3(b) that the RMSEs for the BPSK signal situations are lower than that of the Gaussian and the QPSK signal situations, indicating that the estimating performance of our proposed algorithm for noncircular signals is better than that for circular signals.

5.2. Estimation accuracy

In the following simulations, we assume two BPSK signals independent of each other and of the same power impinge on 3 array sensors. In Section 5.2, for all the experiments except for the one that the angle separation varies, the two angles of arrival are set to be $\theta_1=-30^\circ$ and $\theta_2=-20^\circ$. Two quantities, namely, the resolution probability and the RMSE averaged for the two sources, are utilized to assess the relative resolution capability and estimation accuracy of EXC-NC-MUSIC and NC-MUSIC.

The two signals are considered to be resolvable if the following resolution criterion holds [18]

$$\Lambda(\theta_1,\theta_2)\triangleq f(\theta_m)-\frac{1}{2}\{f(\theta_1)+f(\theta_2)\}>0 \tag{25}$$

where θ_1 and θ_2 are the two arrival angles for the two sources, $\theta_m=(\theta_1+\theta_2)/2$ is the mid-range between them. Probability of resolution is the ratio of the number of successful runs to the total number of the MC runs.

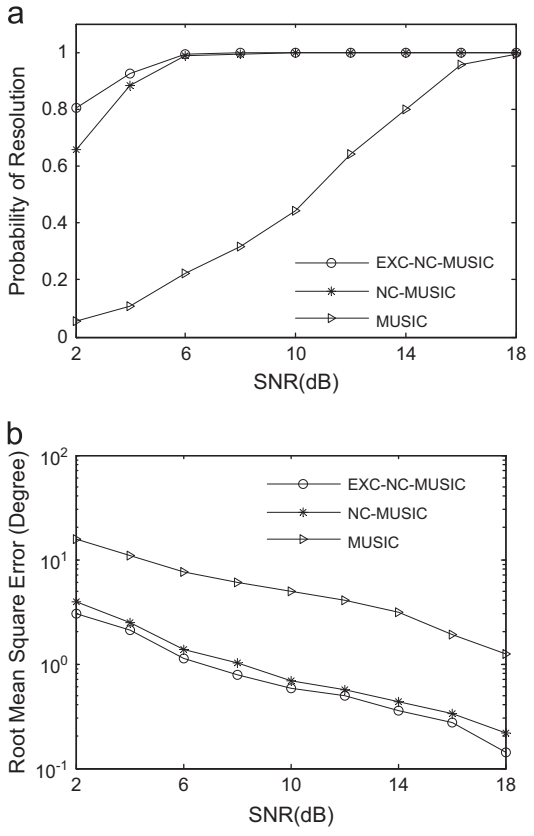

Fig. 4. Performance comparison as a function of SNR condition under Gaussian noise. (a) Probability of resolution and (b) root mean square error.

The simulations compare the performance of EXC-NC-MUSIC and NC-MUSIC as a function of four parameters, namely, the GSNR, the characteristic exponent α of the noise, the angular separation of the two sources, and the number of the snapshots available at the sensors.

5.2.1. Gaussian noise

Fig. 4 illustrates the performance of EXC-NC-MUSIC versus NC-MUSIC and the traditional MUSIC under the scenario of Gaussian noise. The SNR conditions are changing for a wide range from 2 dB to 18 dB. The number of data samples used in the simulation for each sensor is 300. As expected, the traditional MUSIC algorithm exhibits poor performance both in resolution probability and in RMSE especially in low SNR circumstances. By contrast, both EXC-NC-MUSIC and NC-MUSIC gain much better performance as they incorporate the covariance function with the conjugated covariance function for the sensor outputs. Moreover, we can also observe that the running curves of EXC-NC-MUSIC and NC-MUSIC are nearly overlapped which would suggest that EXC-NC-MUSIC yield equivalent performance with NC-MUSIC under Gaussian noise environments.

5.2.2. The effect of the GSNR

Fig. 5 demonstrates the performance comparison of EXC-NC-MUSIC and NC-MUSIC under $S\alpha S$ noise environments. Two noise conditions with the α taking values $\alpha=1.6$ and $\alpha=1.8$ which correspond to moderate

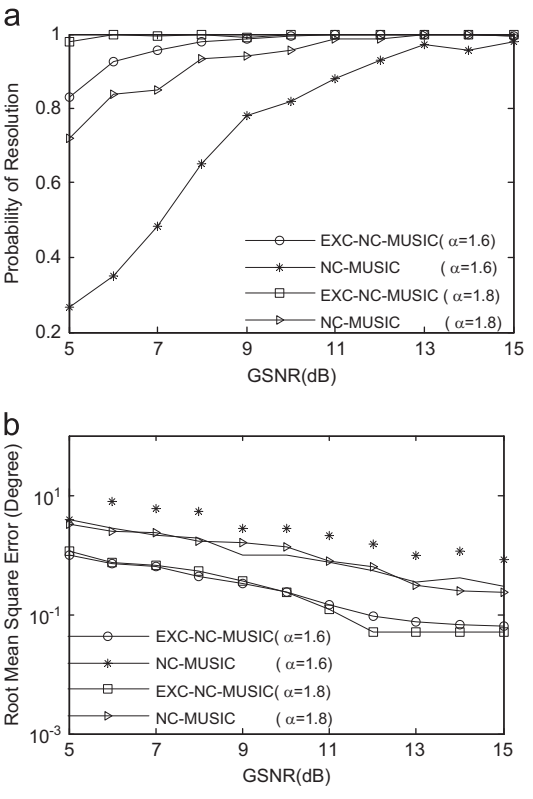

Fig. 5. Performance comparison as a function of GSNR under $S\alpha S$ noise conditions. (a) Probability of resolution and (b) root mean square error.

impulsive and slightly impulsive noise situations respectively, are employed. The GSNR is set to be changing from 5 dB to 15 dB. The number of data samples used in the simulation for each sensor is 300. It is obvious from Fig. 5 that EXC-NC-MUSIC outperforms NC-MUSIC both in terms of resolution probability and RMSE.

5.2.3. The effect of the characteristic exponent α

Fig. 6 illustrates the overall performance of EXC-NC-MUSIC and NC-MUSIC as the characteristic exponent α of the underlying noise varies from 1.1 to 2, corresponding to the transition from extremely impulsive to Gaussian noise conditions. Two GSNR conditions (8 dB and 10 dB) are utilized. The number of data samples used in the simulations for each sensor is 300. As expected, for nearly Gaussian noise environments ($\alpha \geq 1.9$), both EXC-NC-MUSIC and NC-MUSIC can achieve high resolution probabilities and low RMSEs. However, for highly impulsive noise conditions ($\alpha < 1.4$), EXC-NC-MUSIC displays a superior performance both in terms of resolution probability and RMSE.

5.2.4. The effect of the angular separation

Fig. 7 shows the performance of EXC-NC-MUSIC and NC-MUSIC with respect to the angle separation of the two incoming signals. A fairly impulsive noise situation with $\alpha = 1.6$ is involved in the simulation. The GSNR is set as 12 dB. The number of data samples available at each sensor is 300. As we can see from Fig. 7 that, for a given angle separation, the EXC-NC-MUSIC algorithm always achieves much higher resolution probability and lower RMSE than NC-MUSIC does. Another interesting observation from Fig. 7 is that the RMSE of NC-MUSIC does not demonstrate an evident descent even when the angular separation increases, indicating that NC-MUSIC does not adapt to the impulsive noise environments.

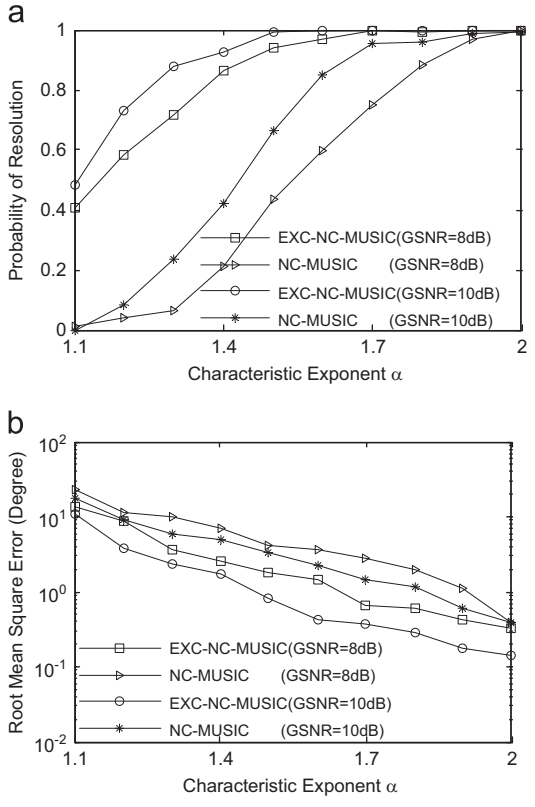

Fig. 6. Performance comparison as a function of characteristic exponent α. (a) Probability of resolution and (b) root mean square error.

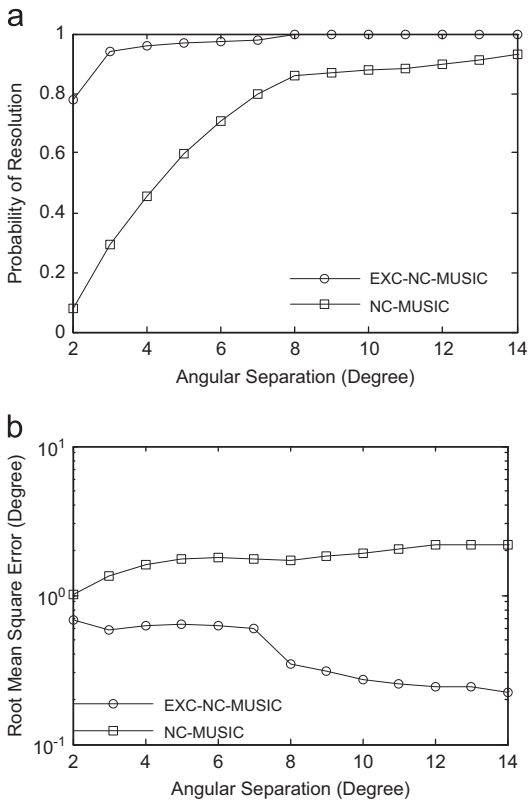

Fig. 7. Performance comparison as a function of the angular separation. (a) Probability of resolution and (b) root mean square error.

5.2.5. The effect of the snapshots

Fig. 8 illustrates how the number of the snapshots K affects the performance of EXC-NC-MUSIC and NC-MUSIC algorithms. A moderate impulsive noise situation with $\alpha = 1.6$ is employed. The GSNR is set to be 10 dB. From Fig. 8 we can see that, with the increase of the number of snapshots, more and more impulsive noise samples are incorporated into the data, the NC-MUSIC displays a distinct deterioration both in the resolution probability and in the RMSE. By contrast, the performance of EXC-NC-MUSIC illustrates a consistent improvement along with the increase of the number of snapshots.

5.3. Noncircular $S\alpha S$ signals

As previously demonstrated, the simulations in Sections 5.1 and 5.2 are executed under the assumption that the noise is $S\alpha S$ distributed. Meanwhile, the signals' types are those frequently encountered ones in practical communications applications, such as BPSK, QPSK, Gaussian, etc. However, our proposed algorithm is not limited to communication

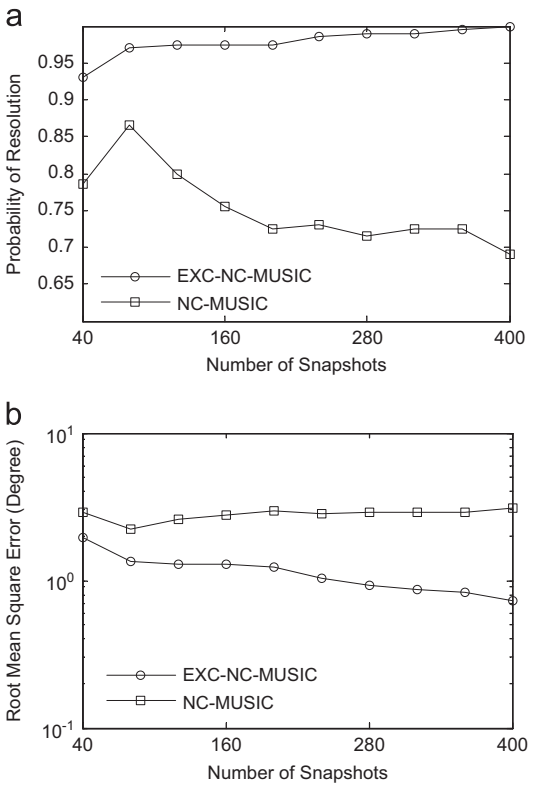

Fig. 8. Performance comparison as a function of the number of snapshots. (a) Probability of resolution and (b) root mean square error.

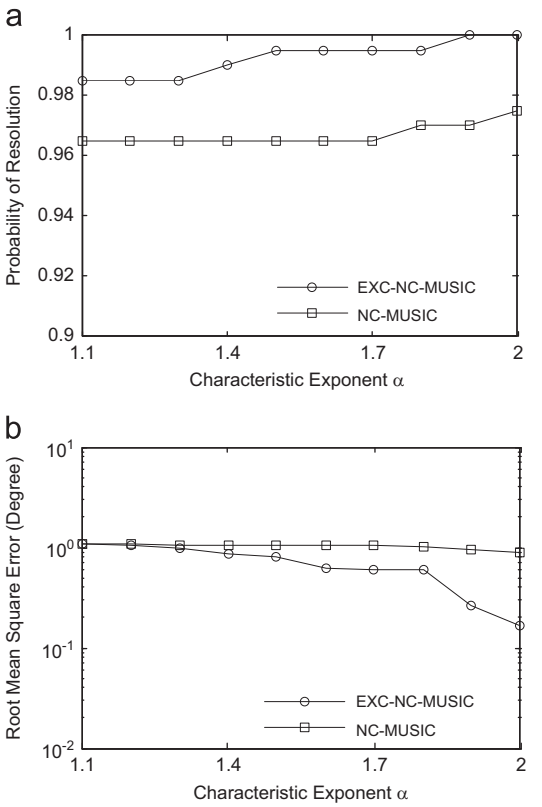

Fig. 9. Performance of EXC-NC-MUSIC under noncircular $S\alpha S$ signals. (a) Probability of resolution and (b) root mean square error.

applications. To further examine the robustness of EXC-NC-MUSIC and to give some references for other possible applications, in the following simulation, we assume that the signals and noise are both $S\alpha S$ distributed. A moderate impulsive noise environment is employed by setting the characteristic exponent $\alpha=1.6$ and the GSNR is set at 15 dB. Fig. 9 demonstrates the performance of EXC-NC-MUSIC and NC-MUSIC as the characteristic exponent α of the noncircular $S\alpha S$ signals varies from 1.1 to 2.0. From Fig. 9 we can observe that, the performance of EXC-NC-MUSIC displays an overall improvement than that of NC-MUSIC as the characteristic exponent α of the signals increases.

For analysis convenience, in this paper, the signals and the noise are both assumed to be i.i.d. isotropic complex $S\alpha S$ random processes and are with the same characteristic exponent α as well. However, it should be noted that EXC-NC-MUSIC is not limited to estimating DOAs from noncircular $S\alpha S$ sources. The robust performance of EXC-NC-MUSIC for not only $S\alpha S$ signals but also those frequently encountered communication signals, such as BPSK, QPSK, Gaussian sources, has been shown by the comprehensive simulation results in Sections 5.1–5.3. This robust behavior inspires us that it is beneficial to directly employ EXC-NC-MUSIC for DOA estimation applications under highly impulsive environments.

5.4. Selection of the parameter p

The principle of the robustness of EXC-NC-MUSIC for $S\alpha S$ noise environments lies in it applying covariation functions instead of covariance functions to formulate the corresponding extended covariation matrix for the array outputs. The operation $(\cdot)^{\langle p-1\rangle}$ in covariation restrains the amplitude of the outliers but preserves the phase information as well, that is, the robustness of EXC-NC-MUSIC depends on the appropriate selection of p.

In the following simulation, we assume two BPSK signals independent of each other and of the same power impinge on 3 array sensors. The two angles of arrival are set to be $\theta_1=-30^\circ$ and $\theta_2=-20^\circ$. The performance of EXC-NC-MUSIC as a function of the parameter p is demonstrated in Fig. 10. The interval [0.2 2] for p is considered in the simulation inspired by the definition of MFLOM. Four noise conditions are set to be $\alpha=1.6$, GSNR=5 dB; $\alpha=1.6$, GSNR=10 dB; $\alpha=1.8$, GSNR=5 dB; and $\alpha=1.8$, GSNR=10 dB. From Fig. 10 we can observe that the performance of EXC-NC-MUSIC deteriorates evidently for $p\ \alpha$ and $p<0.5$. On the contrary, EXC-NC-MUSIC using p close to 1 always gives fairly better performance, in terms of higher resolution probability and lower RMSE. Considering that the value of α is often not easy to evaluate in priori in real applications especially in the case that the value of α dynamically changes, we can choose $p=1$ directly.

6. Conclusion

By exploiting the potential of the noncircular signals, we have formulated the extended covariation matrix of the array output for the case of complex isotropic $S\alpha S$

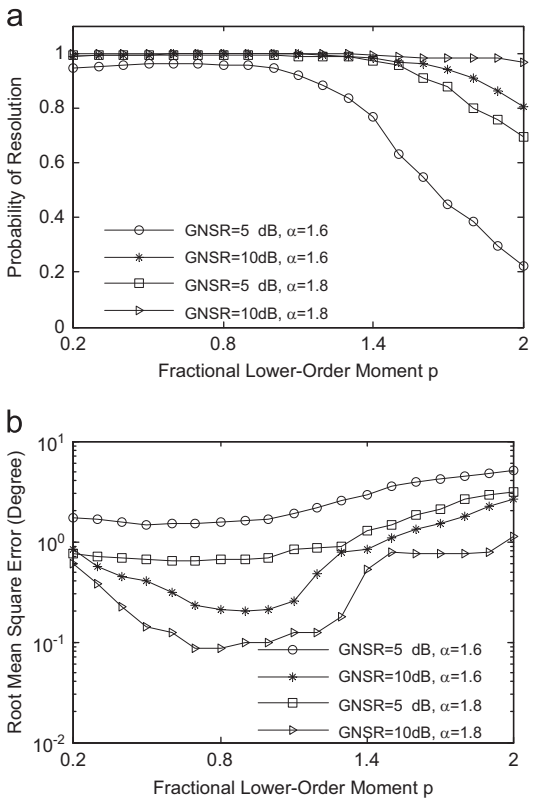

Fig. 10. Performance of EXC-NC-MUSIC as a function of the parameter p. (a) Probability of resolution and (b) root mean square error.

noncircular signals and noise. We show that, the extended covariation matrix has similar form to the extended covariance matrix in NC-MUSIC for Gaussian distributed noncircular signals and noise. Through minimizing the corresponding EXC-NC-MUSIC spatial spectrum, we can obtain the DOA estimates in the presence of impulsive noise environments. Simulation results demonstrate the performance improvement of EXC-NC-MUSIC over NC-MUSIC algorithm for impulsive noise situations. We discuss the selection of the parameter p in EXC-NC-MUSIC, and conclude that the proposed algorithm with p close to 1 yields good performance when the impulsive noise is $S\alpha S$ with unknown α.

Acknowledgments

The authors acknowledge the support from National Natural Science Foundation of China under Grants 60872122, 61172108, 61139001 and 81241059, and would like to thank the anonymous reviewers for their useful comments and suggestions that significantly improved the paper.

Appendix A

Proof of Theorem 1

As shown in Eq. (15), the $2M\times 2M$ extended covariation matrix $\mathbf{C}_{nc}$ of the extended output vector $\mathbf{x}_{nc}(t)$ can be divided into four $M\times M$ sub-matrices: $\mathbf{C}^1$,$\mathbf{C}^2$,$\mathbf{C}^3$, and $\mathbf{C}^4$, and the corresponding (i,j)th entries of these four sub-matrices are taking the values $[x_i(t),x_j(t)]_\alpha$, $[x_i(t),x_j^*(t)]_\alpha$, $[x_i^*(t),x_j(t)]_\alpha$ and $[x_i^*(t),x_j^*(t)]_\alpha$, respectively.

$$\mathbf{C}_{\mathrm{nc}}=\begin{bmatrix}\mathbf{C}^1 & \mathbf{C}^2\\ \mathbf{C}^3 & \mathbf{C}^4\end{bmatrix} \tag{26}$$

Let $C_{ij}^1=[x_i(t),x_j(t)]_\alpha$, $C_{ij}^2=[x_i(t),x_j^*(t)]_\alpha$, $C_{ij}^3=[x_i^*(t),x_j(t)]_\alpha$ and $C_{ij}^4=[x_i^*(t),x_j^*(t)]_\alpha$. In the following content, we will analyze the four entries C_{ij}^1, C_{ij}^2, C_{ij}^3, and C_{ij}^4 sequentially.

Using the independence assumption between the signal $\mathbf{s}(t)$ and the noise $\mathbf{n}(t)$ and by the properties of covariation, we have that

$$\begin{aligned}C_{ij}^1&=[x_i(t),x_j(t)]_\alpha\\&=[\mathbf{A}_i(\theta)\mathbf{s}(t)+n_i(t),\mathbf{A}_j(\theta)\mathbf{s}(t)+n_j(t)]_\alpha\\&=[\mathbf{A}_i(\theta)\mathbf{s}(t),\mathbf{A}_j(\theta)\mathbf{s}(t)]_\alpha+[n_i(t),n_j(t)]_\alpha\end{aligned} \tag{27}$$

where $\mathbf{A}_i(\theta)=[e^{-j(2\pi/\lambda)d(i-1)\sin(\theta_1)},e^{-j(2\pi/\lambda)d(i-1)\sin(\theta_2)},\ldots,e^{-j(2\pi/\lambda)d(i-1)\sin(\theta_P)}]\quad i=1,2,\ldots,M$.

By using the expression of the signal $\mathbf{s}(t)$ in Eq. (13), the independent assumption of the signals, and the properties P1 and P2 for covariation, it follows that

$$[\mathbf{A}_i(\theta)\mathbf{s}(t),\mathbf{A}_j(\theta)\mathbf{s}(t)]_\alpha=\left[\sum_{k=1}^{P}a_i(\theta_k)e^{j\phi_k/2}s_{0k}(t),\sum_{l=1}^{P}a_j(\theta_l)e^{j\phi_l/2}s_{0l}(t)\right]_\alpha$$

$$=\sum_{k=1}^{P}a_i(\theta_k)e^{j\phi_k/2}(a_j(\theta_k)e^{j\phi_k/2})^{\langle\alpha-1\rangle}[s_{0k}(t),s_{0k}(t)]_\alpha \tag{28}$$

As the steering vector $\mathbf{a}(\theta_k)$ is of the form $\mathbf{a}(\theta_k)=[1,e^{-j(2\pi/\lambda)d\sin(\theta_k)},\ldots,e^{-j(2\pi/\lambda)d(M-1)\sin(\theta_k)}]^T$, and from the formula $Y^{\langle b\rangle}=|Y|^{b-1}Y^*$, we have that

$$(a_j(\theta_k)e^{j\phi_k/2})^{\langle\alpha-1\rangle}=a_j^*(\theta_k)e^{-j\phi_k/2} \tag{29}$$

Therefore, the first item of the summation in (27) can be further expressed as

$$\begin{aligned}[\mathbf{A}_i(\theta)\mathbf{s}(t),\mathbf{A}_j(\theta)\mathbf{s}(t)]_\alpha&=\sum_{k=1}^{P}a_i(\theta_k)a_j^*(\theta_k)[s_{0k}(t),s_{0k}(t)]_\alpha\\&=\sum_{k=1}^{P}a_i(\theta_k)a_j^*(\theta_k)\gamma_{0k}\end{aligned} \tag{30}$$

in which $\gamma_{0k}=[s_{0k}(t),s_{0k}(t)]_\alpha\quad k=1,2,\ldots,P$.

Also, due to the noise assumption it holds that

$$[n_i(t),n_j(t)]_\alpha=\kappa_n\delta_{i,j} \tag{31}$$

where $\delta_{i,j}$ is the Kronecker delta function and $\kappa_n=[n_i(t),n_i(t)]_\alpha$.

Combining (30) with (31), we have

$$\begin{aligned}C_{ij}^1&=[x_i(t),x_j(t)]_\alpha\\&=\sum_{k=1}^{P}a_i(\theta_k)a_j^*(\theta_k)\gamma_{0k}+\kappa_n\delta_{i,j}\end{aligned} \tag{32}$$

Similarly, the analysis of C_{ij}^2 which stands for the (i,j)th entry of the sub-matrix $\mathbf{C}^2$ can be obtained as follows.

$$\begin{aligned} C_{ij}^2 &= [x_i(t), x_j^*(t)]_\alpha \\ &= [\mathbf{A}_i(\theta)\mathbf{s}(t)+n_i(t), \mathbf{A}_j^*(\theta)\mathbf{s}^*(t)+n_j^*(t)]_\alpha \\ &= [\mathbf{A}_i(\theta)\mathbf{s}(t), \mathbf{A}_j^*(\theta)\mathbf{s}^*(t)]_\alpha + [n_i(t), n_j^*(t)]_\alpha \end{aligned} \tag{33}$$

Utilizing the expression of the signal $\mathbf{s}(t)$ in (13) and the properties of covariation, it follows that

$$\begin{aligned} &[\mathbf{A}_i(\theta)\mathbf{s}(t), \mathbf{A}_j^*(\theta)\mathbf{s}^*(t)]_\alpha \\ &= \left[\sum_{k=1}^{P} a_i(\theta_k)e^{j\phi_k/2}s_{0k}(t), \sum_{l=1}^{P} a_j^*(\theta_l)e^{-j\phi_l/2}s_{0l}(t)\right]_\alpha \\ &= \sum_{k=1}^{P} a_i(\theta_k)e^{j\phi_k/2}(a_j^*(\theta_k)e^{-j\phi_k/2})^{\langle\alpha-1\rangle}[s_{0k}(t), s_{0k}(t)]_\alpha \\ &= \sum_{k=1}^{P} a_i(\theta_k)a_j(\theta_k)e^{j\phi_k}\gamma_{0k} \end{aligned} \tag{34}$$

Also, due to the noise assumption it holds that

$$[n_i(t), n_j^*(t)]_\alpha = \begin{cases} 0 & i \neq j \\ [n_i(t), n_i^*(t)]_\alpha & i = j \end{cases} \tag{35}$$

in which

$$\begin{aligned} [n_i(t), n_i^*(t)]_\alpha &= [\Re(n_i(t))+j\Im(n_i(t)), \Re(n_i(t))-j\Im(n_i(t))]_\alpha \\ &= [\Re(n_i(t)), \Re(n_i(t))]_\alpha + j(-j)^{\langle\alpha-1\rangle}[\Im(n_i(t)), \Im(n_i(t))]_\alpha \\ &= 0 \end{aligned} \tag{36}$$

here, the independence assumption between $\Re(n_i(t))$ and $\Im(n_i(t))$ is applied. From the above analysis, we have

$$C_{ij}^2 = \sum_{k=1}^{P} a_i(\theta_k)a_j(\theta_k)e^{j\phi_k}\gamma_{0k} \tag{37}$$

Implementing the similar analysis on C_{ij}^3 and C_{ij}^4 with that on C_{ij}^2 and C_{ij}^1, we have

$$C_{ij}^3 = \sum_{k=1}^{P} a_i^*(\theta_k)a_j^*(\theta_k)e^{-j\phi_k}\gamma_{0k} \tag{38}$$

and

$$C_{ij}^4 = \sum_{k=1}^{P} a_i^*(\theta_k)a_j(\theta_k)\gamma_{0k} + \kappa_n\delta_{i,j} \tag{39}$$

Thus, incorporating C_{ij}^2, C_{ij}^3, and C_{ij}^4 with C_{ij}^1, we have $\mathbf{C}_{nc}$ expressed in (16). □

Appendix B

Derivation of the 1-D spatial spectrum f(θ) for NC-MUSIC

As shown in (20), the DOA estimates can be derived by minimizing the following spatial spectrum $g(\theta,\phi)$ over θ and ϕ

$$g(\theta,\phi) = \mathbf{b}^H(\theta,\phi)\mathbf{V}_n\mathbf{V}_n^H\mathbf{b}(\theta,\phi) \tag{40}$$

where $\mathbf{b}(\theta_i,\phi_i) = [\mathbf{a}(\theta_i) \quad \mathbf{a}^*(\theta_i)e^{-j\phi_i}]^T \quad i = 1,2,\ldots,P$ are the extended steering vectors, and $\mathbf{V}_n$ are the corresponding left singular vectors associated with the noise subspace of the extended covariation matrix $\mathbf{C}_{nc}$. Since the directions of arrival $\{\theta_1,\theta_2,\ldots,\theta_P\}$ are our concern, to alleviate the computational complexity, it is necessary to transform the 2-D search over θ and ϕ to the 1-D search only over θ. The technique can be expressed as follows [4].

Partitioning $\mathbf{V}_n$ into two sub-matrices $\mathbf{V}_{n1}$ and $\mathbf{V}_{n2}$ which have the same dimensions as

$$\mathbf{V}_n = \begin{bmatrix} \mathbf{V}_{n1} \\ \mathbf{V}_{n2} \end{bmatrix} \tag{41}$$

we have

$$\begin{aligned} g(\theta,\phi) &= \mathbf{b}^H(\theta,\phi)\begin{bmatrix} \mathbf{V}_{n1} \\ \mathbf{V}_{n2} \end{bmatrix}\begin{bmatrix} \mathbf{V}_{n1}^H & \mathbf{V}_{n2}^H \end{bmatrix}\mathbf{b}(\theta,\phi) \\ &= \mathbf{b}^H(\theta,\phi)\begin{bmatrix} \mathbf{V}_{n1}\mathbf{V}_{n1}^H & \mathbf{V}_{n1}\mathbf{V}_{n2}^H \\ \mathbf{V}_{n2}\mathbf{V}_{n1}^H & \mathbf{V}_{n2}\mathbf{V}_{n2}^H \end{bmatrix}\mathbf{b}(\theta,\phi) \end{aligned} \tag{42}$$

Substituting $\mathbf{b}(\theta,\phi)$ with $\begin{bmatrix} \mathbf{a}(\theta) & \mathbf{a}^*(\theta)e^{-j\phi_i} \end{bmatrix}^T$ in (42), we find that

$$\begin{aligned} g(\theta,\phi) &= [\mathbf{a}^H(\theta) \quad (\mathbf{a}^*(\theta))^H e^{j\phi}]\begin{bmatrix} \mathbf{V}_{n1}\mathbf{V}_{n1}^H & \mathbf{V}_{n1}\mathbf{V}_{n2}^H \\ \mathbf{V}_{n2}\mathbf{V}_{n1}^H & \mathbf{V}_{n2}\mathbf{V}_{n2}^H \end{bmatrix}\begin{bmatrix} \mathbf{a}(\theta) \\ \mathbf{a}^*(\theta)e^{-j\phi} \end{bmatrix} \\ &= [1 \quad e^{j\phi}]\begin{bmatrix} \mathbf{a}^H(\theta) & \mathbf{0} \\ \mathbf{0} & (\mathbf{a}^*(\theta))^H \end{bmatrix}\begin{bmatrix} \mathbf{V}_{n1}\mathbf{V}_{n1}^H & \mathbf{V}_{n1}\mathbf{V}_{n2}^H \\ \mathbf{V}_{n2}\mathbf{V}_{n1}^H & \mathbf{V}_{n2}\mathbf{V}_{n2}^H \end{bmatrix} \\ &\quad \times \begin{bmatrix} \mathbf{a}(\theta) & \mathbf{0} \\ \mathbf{0} & \mathbf{a}^*(\theta) \end{bmatrix}\begin{bmatrix} 1 \\ e^{-j\phi} \end{bmatrix} \end{aligned} \tag{43}$$

Solving the partial differential equation $(\partial g(\theta,\phi)/\partial\phi) = 0$, we have

$$e^{j\phi} = \pm\frac{\mathbf{a}^H(\theta)\mathbf{V}_{n1}\mathbf{V}_{n2}^H\mathbf{a}^*(\theta)}{\|\mathbf{a}^H(\theta)\mathbf{V}_{n1}\mathbf{V}_{n2}^H\mathbf{a}^*(\theta)\|} \tag{44}$$

Check the two values that $e^{j\phi}$ can take in (44), we can deduce that the one with the minus sign in (44) results in the minimum for $g(\theta,\phi)$, and the minimum is

$$\begin{aligned} f(\theta) &= \mathbf{a}^H(\theta)\mathbf{V}_{n1}\mathbf{V}_{n1}^H\mathbf{a}(\theta) + \mathbf{a}^T(\theta)\mathbf{V}_{n2}\mathbf{V}_{n2}^H\mathbf{a}^*(\theta) \\ &\quad - 2\|\mathbf{a}^H(\theta)\mathbf{V}_{n1}\mathbf{V}_{n2}^H\mathbf{a}^*(\theta)\| \end{aligned} \tag{45}$$

Evidently, the 2-D search by minimizing the spatial spectrum $g(\theta,\phi)$ over θ and ϕ in (40) can be simplified as the 1-D search only over θ for the local minima of the spatial spectrum $f(\theta)$ in (45).

Appendix C

The mathematical description of BPSK, QPSK, Gaussian signals, and the generation of circular and noncircular $S\alpha S$ signals

We can express the signal $s_k(t)$ as $s_k(t) = u_k(t)e^{j\psi_k(t)}$, where amplitude $u_k(t)$ and phase $\psi_k(t)$ are two sequences of real random variables that are statistically independent of each other. The signal types appeared in our simulations can be interpreted as follows:

(1) BPSK: $u_k(t)$ is a constant, $\psi_k(t)$ is a sequence of i.i.d random variables that are uniformly taking values 0 and π.
(2) QPSK: $u_k(t)$ is a constant, $\psi_k(t)$ is a sequence of i.i.d random variables that are uniformly taking values $(\pi/4)$, $(3\pi/4)$, $(5\pi/4)$ and $(7\pi/4)$.
(3) Symmetrical Gaussian: $u_k(t)$ is Rayleigh-distributed, $\psi_k(t)$ is a sequence of i.i.d random variables that are uniform over $[0 \quad 2\pi]$.

Based on the principles of circularity (refer to Section 3.2), it is easy to conclude that QPSK and Gaussian signals are circular, while BPSK is noncircular.

Similarly, we generated circular and noncircular $S\alpha S$ signals as follows:

(4) Circular $S\alpha S$ signal: $u_k(t)$ is real $S\alpha S$ distributed random variables, $\psi_k(t)$ is a sequence of i.i.d random variables that are uniform over [0 2π].

(5) Noncircular $S\alpha S$ signal: $u_k(t)$ is real $S\alpha S$ distributed random variables, $\psi_k(t)$ is a sequence of i.i.d random variables that are uniformly taking values 0 and π.

where the generation of complex isotropic $S\alpha S$ random variables can be found in Ref. [15].

References

[1] D. Johnson, D. Dudgeon, Array Signal Processing: Concepts and Techniques, Prentice-Hall, Englewood Cliffs, NJ, 1993.

[2] R.O. Schmidt, Multiple emitter location and signal parameter estimation, IEEE Trans. Antennas Propagat. 34 (1986) 276–280.

[3] R.R. Mohler, A second-order eigenstructure array processor, in: Proceedings of the Workshop on Higher Order Spectral Analysis, 1989, pp. 152–157.

[4] P. Gounon, C. Adnet, J. Galy, Localization angulaire de signaux non circulaires, Traitement du Signal 15 (1998) 17–23.

[5] P. Chargé, Y. Wang, J. Saillard, A non-circular sources direction finding method using polynomial rooting, Signal Process. 81 (2001) 1765–1770.

[6] M. Haardt, F. Römer, Enhancements of unitary ESPRIT for non-circular sources, IEEE ICASSP, Montreal, QC, Canada, II, 2004, pp. 101–104.

[7] A. Zoubir, P. Chargé, Y. Wang, Non-circular sources localization with ESPRIT, in: Proceedings of the 6th European Conference on Wireless Technology, October 2003.

[8] H. Abeida, J.P. Delmas, MUSIC-like estimation of direction of arrival for noncircular sources, IEEE Trans. Signal Process. 54 (2006) 2678–2690.

[9] J. Liu, Z. Huang, Y. Zhou, Extended 2q-MUSIC algorithm for non-circular signals, Signal Process. 88 (2008) 1327–1339.

[10] K.L. Blackard, T.S. Rappaport, C.W. Bostian, Measurements and models of radio frequency impulsive noise for indoor wireless communications, IEEE J. Sel. Areas Commun. 11 (1993) 991–1001.

[11] M.D. Button, J.G. Gardiner, I.A. Glover, Measurement of the impulsive noise environment for satellite-mobile radio systems at 1.5 GHz, IEEE Trans. Veh. Technol. 51 (2002) 551–560.

[12] A. Ahandra, Measurements of radio impulsive noise from various sources in an indoor environment at 900 MHz and 1800 MHz, in: the 13th IEEE International Symposium on Personal, Indoor and Mobile Radio Communications, vol. 2, 2002, pp. 639–643.

[13] J.H. Miller, Detections for discrete-time signals in non-Gaussian noise, IEEE Trans. Inf. Theory 18 (1972) 241–250.

[14] W. Stuck, B. Kleiner, A statistical analysis of telephone noise, Bell Syst. Tech. J. 53 (1974) 1263–1320.

[15] C.L. Nikias, M. Shao, Signal Processing with α-Stable Distribution and Applications, John Wiley&Sons, New York, NY, 1995.

[16] P. Tsakalides, C.L. Nikias, Robust covariation-based MUSIC (ROC-MUSIC) algorithm for bearing estimation in impulsive noise environments, IEEE Trans. Signal Process. 44 (1996) 1623–1633.

[17] B. Picinbono, On circularity, IEEE Trans. Signal Process. 42 (1994) 3473–3482.

[18] Q.T. Zhang, Probability of resolution of the MUSIC algorithm, IEEE Trans. Signal Process. 43 (1995) 978–987.

[19] T.H. Liu, J.M. Mendel, A subspace-based direction finding algorithm using fractional lower order statistics, IEEE Trans. Signal Process. 49 (2001) 1605–1613.